Communications in Theoretical Physics

Commun. Theor. Phys. **77** (2025) 085403 (12pp) https://doi.org/10.1088/1572-9494/adbc63
CSTR: 32041.14.CTPadbc63

Thermal radiation of accretion disks around a charged Hayward black hole

Munisa Boltatoshova[1], Bakhtiyor Narzilloev[2,3] and Bobomurat Ahmedov[1,2,4,*]

[1] Institute of Theoretical Physics, National University of Uzbekistan, Tashkent 100174, Uzbekistan
[2] Institute for Advanced Studies, New Uzbekistan University, Movarounnahr Str. 1, Tashkent 100000, Uzbekistan
[3] University of Tashkent for Applied Sciences, Str. Gavhar 1, Tashkent 100149, Uzbekistan
[4] Ulugh Beg Astronomical Institute, Astronomy St. 33, Tashkent 100052, Uzbekistan

E-mail: boltatoshovamunisa@gmail.com, b.narzilloev@newuu.uz and ahmedov@astrin.uz

Received 31 October 2024, revised 17 January 2025
Accepted for publication 26 January 2025
Published 28 April 2025

Abstract

This study explores the dynamics of charged Hayward black holes, focusing on the effects of electric charge and the length factor on accretion disk characteristics. Our results show that increasing both parameters reduces the size of the event horizon and innermost stable circular orbits (ISCO) radius, with the electric charge exerting a more pronounced influence. Additionally, the length factor and electric charge can effectively replicate the spin of a Kerr black hole. Both parameters also affect the electromagnetic radiation emitted from the accretion disk, increasing the flux, temperature, and radiative efficiency. The peak radiation occurs in the soft x-ray band, with higher values of electric charge and length factor enhancing disk luminosity and shifting the peak to higher frequencies. These findings can offer valuable insights into the accretion processes around black holes and their observable signatures, particularly in x-ray astronomy.

Keywords: black hole, dark matter, accretion disk, general relativity

(Some figures may appear in colour only in the online journal)

1. Introduction

The renowned singularity theorem posits that, under particular circumstances, the gravitational collapse of sufficiently massive stars results in the creation of black holes with spacetime singularities [1–3]. One of the primary challenges in classical general relativity is the inevitable presence of these singularities. Conventional black hole solutions, such as the Schwarzschild, Reissner–Nordström, and Kerr metrics, inherently display curvature singularities at their cores. This has led to the proposition that classical general relativity might need revisions in regions where spacetime curvature diverges, suggesting that quantum gravity could offer a resolution to these singularities. However, in the absence of a fully developed quantum gravity theory, attempts to address black hole singularities have turned towards regular black hole models, which are grounded in quantum principles. For instance, Sakharov [4] and Gliner [5] suggested that at small r, the Einstein tensor assumes the form $G_{\mu\nu} = \Lambda g_{\mu\nu}$ with $\Lambda \neq 0$, signifying a central de Sitter core characterized by the equation of state $P = -\rho$. This condition effectively establishes an upper limit on the scalar curvature. As a result, the collapsed star stabilizes in a state where the outward de Sitter pressure balances the inward gravitational pull, thereby removing the singularity at the center. In the presence of an event horizon, this leads to what is called a regular black hole. Bardeen [6] introduced the first regular black hole model, which was subsequently shown to be an exact solution to Einstein's field equations when coupled with nonlinear electrodynamics (NED) [7–9]. Since then, a variety of regular black hole models have been formulated and studied [10–15] (for an extensive review, see [16]). The absence of singularities at the center helps to address issues like Hawking radiation and the information loss paradox [17]. Hayward

* Author to whom any correspondence should be addressed.

[18] introduced a model that is particularly effective in analyzing the processes of black hole formation and evaporation, presenting a scenario where a vacuum collapses into a regular black hole. This model can also be derived within the framework of NED. When electric charge is included, the Hayward black hole becomes an intriguing model for examining the interactions between spacetime geometry and electromagnetic fields in regular black hole contexts. Electrically charged Hayward black hole solution involves the length factor l which represents the magnetic charge of a black hole through $g^3 = 2Ml^2$. It is worth mentioning that the magnetic charge of a black hole is usually modeled in the context of theories predicting magnetic monopoles, such as certain solutions in Einstein–Maxwell or Einstein–Gauss–Bonnet gravity. Studies of black hole shadows, such as those of M87* by the Event Horizon Telescope, can provide constraints on the magnetic charge. For example, in the context of the Hayward black hole, magnetic charges g have been constrained to values consistent with the black hole's observed shadow size and shape. Recent analyses, such as those in [19], constrain g for M87* to be less than approximately 1.72 (at 1σ) or 2.12 (at 2σ), normalized to the black hole mass. Furthermore, in [20] it has been demonstrated that the regular black hole solutions proposed by Bardeen, Hayward, and Frolov are consistent with current observational constraints. In contrast, the Reissner–Nordström and Einstein–Maxwell-dilaton black hole solutions, for specific physical charge values, result in shadow radii that fall outside the 1σ confidence interval permitted by the 2017 EHT observations. These models are therefore restricted to the charge ranges $0 < q \lesssim 0.90$ and $0 < q \lesssim 0.95$, respectively.

In this work we attempt to analyze electrically charged Hayward black hole through the exploration of accretion disk properties around it. Accretion disks are a common characteristic of various astrophysical systems. They form when material from a surrounding medium, such as a gas cloud or a companion star, is drawn toward a central object by its gravitational pull-typically a black hole or neutron star. As this material moves closer to the central object, its potential energy is transformed into kinetic energy, and the material gains angular momentum due to its rotational motion around the object. These forces result in the material flattening into a disk-like shape as it orbits the central mass. Accretion is a crucial process for transporting matter, with the potential to release up to 10% of the total energy in such systems. Accretion disks appear in a wide range of environments, including young protostellar systems, binary stars, and the vicinity of supermassive black holes in AGNs. A key application of accretion disk theory lies in exploring black hole characteristics. From an astrophysical standpoint, investigating thin accretion around black holes serves as an effective method for probing the strong gravitational field. By comparing observed data on thin accretion in black hole systems to the predicted thermal spectra, one can acquire important insights into the dynamics of black hole systems and their key characteristics.

One should mention that, there are several methods to explore black hole spacetimes. In our prior studies, e.g. we have systematically examined different spacetime metrics around compact objects, using a variety of techniques [21–32]. Specifically, in this work, we focus on the electromagnetic radiation emitted from the disk around charged Hayward black hole due to thermal radiation. Our investigation centers on the Novikov–Thorne framework, characterizing a disk that is both geometrically thin and optically thick. In this study, we also provide the temperature profiles and spectral energy distributions for a thin Novikov–Thorne disk and compare these outcomes to those derived from Kerr black hole spacetime within the context of general relativity.

The layout of this paper is as follows. In section 2, we explore the characteristics of the spacetime surrounding a non-rotating Hayward black hole with electric charge. Section 3 introduces the Novikov–Thorne model for a geometrically thin, optically thick accretion disk around charged Hayward black hole. In section 4, we investigate the energy flux across the disk, its radiative efficiency, temperature distribution, and the emitted radiation spectrum caused by thermal radiation. Lastly, in section 5, we provide a summary of the key findings of the study.

Throughout this paper, we take the gravitational constant and the speed of light to be $G = c = 1$, with a spacetime signature of $(-,+,+,+)$. Greek letters represent four-dimensional spacetime coordinates.

2. Electrically charged Hayward black hole

The line element for the electrically charged Hayward black hole (hereafter, ECH BH) can be written in the following way according to [33]

$$\mathrm{d}s^2 = -f(r)\mathrm{d}t^2 + f(r)^{-1}\mathrm{d}r^2 + r^2(\mathrm{d}\theta^2 + \sin^2\theta\mathrm{d}\phi^2), \quad (1)$$

$$f(r) = 1 - \frac{(2Mr - Q^2)r^2}{r^4 + (2Mr + Q^2)l^2}, \quad (2)$$

where Q stands for electric charge, M for mass and l for a length factor strictly connected with the magnetic charge through the following relation $g^3 = 2Ml^2$. It can be easily checked that when the length factor vanishes, $l \to 0$ the metric recovers Reissner–Nordström solution. One can plot the radial profile of the lapse function as in figure 1. The left plot is for the fixed length factor and different electric charge of a black hole, while the right one is for the fixed electric charge and different length factor. One can see that the effects of both parameters (i.e. Q and l) look almost identical and in the asymptotic infinity recover flat Minkowski spacetime. One can also notice that an increase of both Q and l makes the metric function $f(r)$ bigger in the close vicinity of the central black hole. At the same time, the effects of these parameters are negligible at further distances.

The location of the event horizon can be quickly found from the condition $g^{rr} = 0$. However, it is worth noting here that it does not exist for all the possible values of the spacetime parameters l and Q. In figure 2 we show the parameter space which clearly distinguishes the black hole and no black hole regions separated by the blue solid line. From the plot it is apparent that in the absence of l the

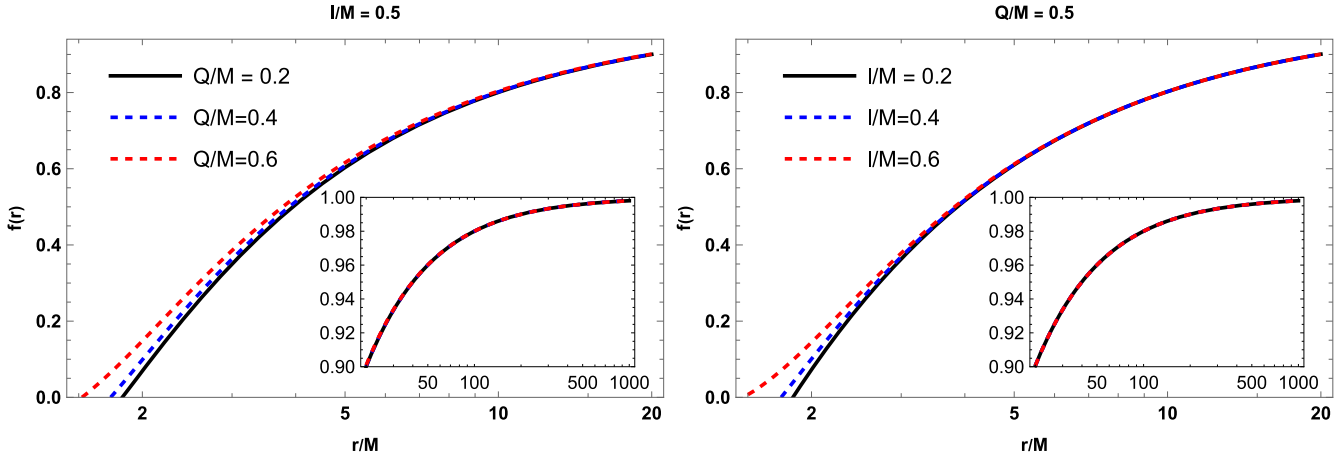

Figure 1. Dependence of lapse function from the radial coordinate for different values of spacetime parameters. In the left plot, parameter *l/M* is set to 0.5, while in the right plot the normalized electric charge *Q/M* is fixed as 0.5.

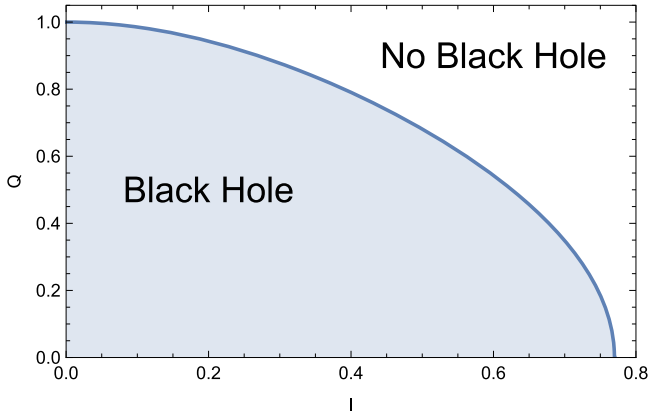

Figure 2. The parameter space of Q and l showing black hole and no black hole regions.

absolute value of the electric charge of a black hole can be at most $Q_{\max} = M$ as in the case of the Reissner–Nordström black hole. In the presence of l, however, the maximum possible absolute value of electric charge for which we still have a black hole solution reduces and approaches zero when l/M approaches ~ 0.77. Now, we can directly solve equation $g^{rr} = 0$ to find the location of the event horizon which is shown with solid lines in the top panels of figure 3 in comparison with the event horizon of the Kerr solution (dashed gray line). It is clearly demonstrated that an increase in both parameters reduces the size of the event horizon in a similar way, with the electric charge having a slightly stronger influence. It is also noticeable that, in the absence of l, the equation $g^{rr} = 0$ becomes exactly the same as that of Kerr spacetime, with the only difference being that the spin of the Kerr black hole, a, is replaced by the electric charge of the static black hole. Therefore we have matching black solid and dashed gray lines in the top-right panel of figure 3. Now one can check how the ECH BH can replicate the Kerr spacetime for the same event horizon structure as shown in the bottom panels of figure 3. From the bottom-left panel, it is clearly seen that the length factor itself can mimic the spin up to $a \simeq 0.93$ which corresponds to the rapidly rotating black hole. The increase of the electric charge of the ECH BH can increase the maximum spin that can be replicated by the length factor but the lowest spin that can be replicated increases. In the bottom-right panel it is clearly demonstrated that the electric charge of the ECH BH can replace the spin completely for the matching event horizon radius which we have already discussed previously. The presence of the length factor reduces the maximum value of electric charge needed to mimic the maximum spin of Kerr black hole but increases the minimum spin that can be replicated. In principle, the effects of the length factor and electric charge on the horizon of a black hole look very similar to each other with small deviations.

3. Thin accretion disk model of Novikov and Thorne

The model of Novikov and Thorne [34, 35] is the conventional framework for modeling accretion disks that are geometrically thin and optically thick. It is a relativistic extension of the earlier Shakura–Sunyaev model [36]. This model, known for its relative simplicity, is developed within a generic stationary, axisymmetric, and asymptotically flat spacetime framework. The time-averaged radial structure of the accretion disk is derived based on the fundamental principles of the conservation of rest mass, energy, and angular momentum. The vertical thickness of the disk is much smaller than its radial extent, with the disk's height h denoting the maximum vertical half-thickness and the radial coordinate r fulfilling $h \ll r$ at every radius. Consequently, the effects of the pressure gradient and vertical entropy gradient in the accreting matter are negligible. A steady-state accretion disk assumes a constant mass accretion rate, denoted by $\dot{M}_0$, over time. This implies that the amount of material entering the disk per unit time is stable, leading to a relatively unchanging disk structure and properties over extended periods.

Steady-state accretion disks are particularly useful for examining matter behavior in extreme environments, such as those surrounding black holes or near young stars. By assuming a constant mass accretion rate, scientists can employ mathematical models to analyze the physical processes within the disk, including the dynamics of the material

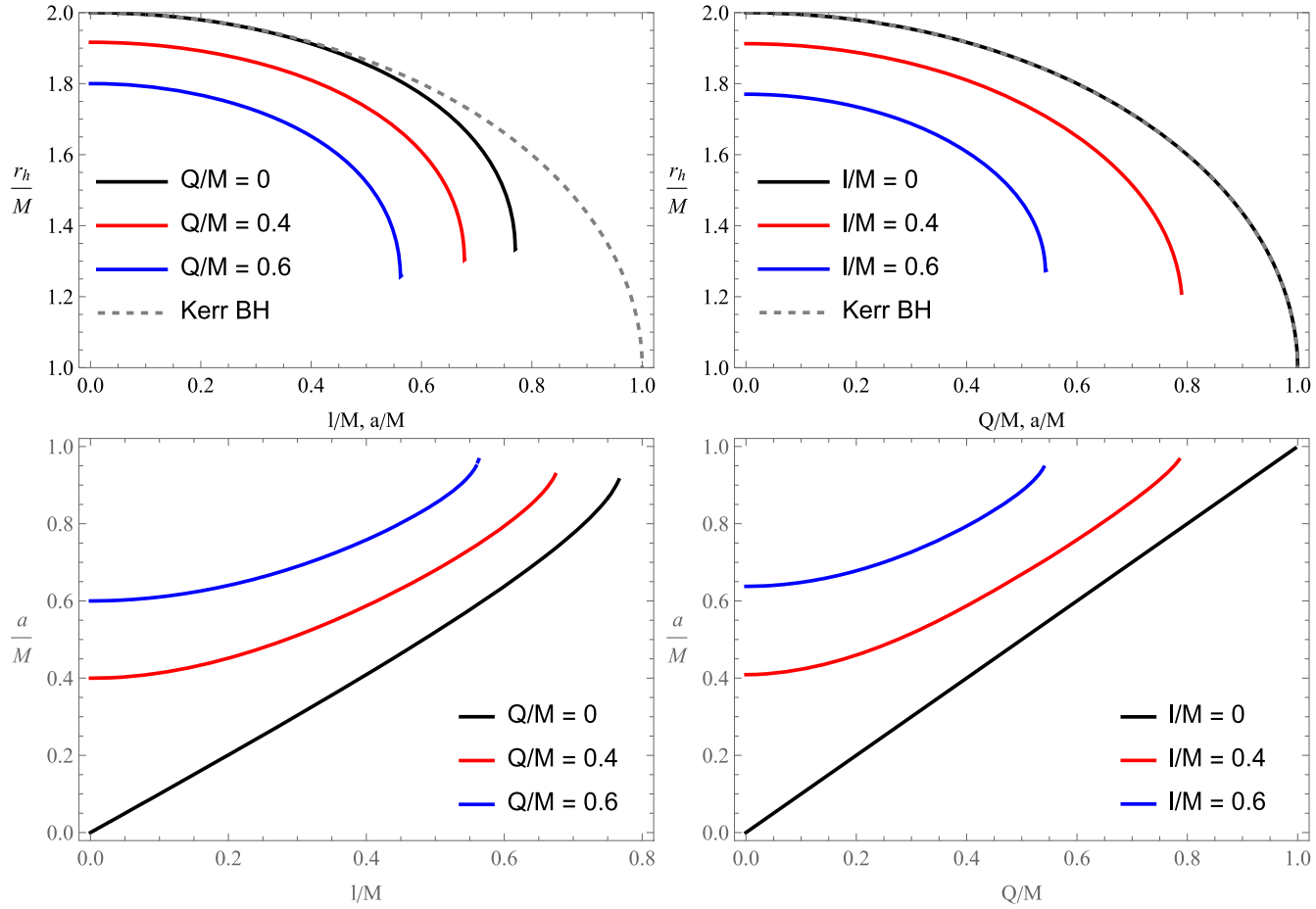

Figure 3. The dependence of the event horizon radius (black solid line), the ISCO radius of the ECH BH (red dashed line), and the ISCO radius of the Kerr BH (blue dashed line) from spacetime parameters.

and the radiation it emits. Despite their apparent simplicity, steady-state accretion disk models have proven to be essential tools in astrophysical research.

The disk dissipates heat efficiently through thermal radiation emitted from its surface, counteracting the heat generated by stresses and dynamic friction. This cooling process is essential for maintaining the disk's thin vertical structure in equilibrium. In astrophysical accretion disks, the inner edge represents a key boundary region that significantly affects the disk's behavior, typically located near a compact object like a black hole or neutron star, which exerts intense gravitational forces on the surrounding matter.

At the inner edge of a thin disk, the material may orbit the compact object at nearly the speed of light due to its rapid movement. This region is known as the marginally stable orbit, representing the closest distance from the compact object where stable circular orbits can exist. Inside this radius, orbits become unstable, and matter quickly falls toward the compact object. Conversely, in higher orbits within the accretion disk, the accreting plasma follows classical Keplerian motion, adhering to the orbital dynamics laws first described by Johannes Kepler. This implies that the velocity of the material decreases as its distance from the compact object increases, leading to slower disk rotation at larger distances.

The plasma within the accretion disk is characterized by physical quantities averaged over a specific time interval, Δt, corresponding to one complete orbit around the azimuthal angle $\Delta\phi = 2\pi$ and over the vertical height h [34, 35, 37]. The effective potential of a massive particle at the equatorial plane (for $M = 1$) is [34, 35, 38]

$$V_{\rm eff} = -1 + \frac{E^2 g_{\phi\phi} + L^2 g_{tt}}{-g_{tt} g_{\phi\phi}}$$

$$= -1 + \frac{\frac{r^2(2l^2r + (-2+r)r^3 + Q^2(l^2+r^2))^2}{Q^4l^4 + 4l^4r^2 + 4l^2r^5 + (-3+r)r^7 + 2Q^2(2l^4r + r^6 + l^2r^3(1+r))} + \frac{r^4(Q^4l^2 - 4l^2r^2 + r^5 - Q^2(2l^2r + r^4))\left(-1 + \frac{r^2(Q^2+2r)}{r^4 + l^2(Q^2+2r)}\right)}{Q^4l^4 + 4l^4r^2 + 4l^2r^5 + (-3+r)r^7 + 2Q^2(2l^4r + r^6 + l^2r^3(1+r))}}{r^2\left(1 - \frac{r^2(-Q^2+2r)}{r^4 + l^2(Q^2+2r)}\right)},$$

where E and L represent the specific energy and angular momentum of the test particles. These quantities, expressed using the metric components, are given as follows

$$E = \frac{-g_{tt}}{\sqrt{-g_{tt} - \Omega^2 g_{tt}}} = \frac{2l^2 r + (-2+r)r^3 + Q^2(l^2+r^2)}{(Q^2l^2 + 2l^2 r + r^4)\sqrt{\frac{Q^4l^4 + 4l^4r^2 + 4l^2r^5 + (-3+r)r^7 + 2Q^2(2l^4r + r^6 + l^2r^3(1+r))}{(Q^2l^2 + 2l^2r + r^4)^2}}} \quad (3)$$

for the energy and

$$L = \frac{\Omega g_{\phi\phi}}{\sqrt{-g_{tt} - \Omega^2 g_{\phi\phi}}} = \frac{r\sqrt{\frac{r^2(Q^4l^2 - 4l^2r^2 + r^5 - Q^2(2l^2r + r^4))}{(Q^2l^2 + 2l^2r + r^4)^2}}}{\sqrt{\frac{Q^4l^4 + 4l^4r^2 + 4l^2r^5 + (-3+r)r^7 + 2Q^2(2l^4r + r^6 + l^2r^3(1+r))}{(Q^2l^2 + 2l^2r + r^4)^2}}} \quad (4)$$

for the angular momentum. In this context, the angular velocity $\mathrm{d}\phi/\mathrm{d}t$, denoted as Ω, is calculated as

$$\Omega = \frac{\mathrm{d}\phi}{\mathrm{d}t} = \frac{\sqrt{-(g_{\phi\phi,r})(g_{tt,r})}}{g_{\phi\phi,r}} = \frac{\sqrt{\frac{r^2(Q^4l^2 - 4l^2r^2 + r^5 - Q^2(2l^2r + r^4))}{(Q^2l^2 + 2l^2r + r^4)^2}}}{r}. \quad (5)$$

The radial profile of the above functions take place in figure 4. The top panel illustrates variations in the effective potential for a test particle, given fixed specific energy and angular momentum values of this particle. In the second and third rows it is shown that the values of the specific energy and angular momentum of a test particle needed to stay at the selected circular orbit. Finally, in the last row, the change of the angular velocity of a test particle with its radial coordinate is plotted. From the left and right panels of the figure one can easily notice that the effects of the length factor and electric charge of a black hole are very similar to each other where increasing both reduces the value of each quantity.

From the following three conditions

$$V_{\mathrm{eff}}(r) = 0, \quad V'_{\mathrm{eff}}(r) = 0, \quad V''_{\mathrm{eff}}(r), \quad (6)$$

one can find the location of the innermost stable circular orbits (ISCO) of the massive test particles. Numerical results are presented in table 1 and graphical representation in figure 5. In the table 'NB' refers to the no black hole region of the $l - Q$ space.

In the top panels of figure 5, we have shown the relationship between the ISCO radii of the ECH black holes and the spacetime parameters, compared with that of the Kerr black hole. The left panel shows the alteration of the ISCO radius as the length factor varies for different fixed values of the electric charge Q. It is clearly seen that the effect of the length factor on the ISCO radius is very small. In the right panel, the change of the ISCO radius with Q for various l is shown. From the plots, one can notice that the increase of both spacetime parameters l and Q reduces the ISCO radius of the ECH BH similar to the spin of Kerr black hole but in a weaker manner. In this sense one can check how well l and Q can mimic the role of the spin of the Kerr black hole in terms of matching ISCO radius as shown in figure 5. From the left plot, one can see that in the absence of the electric charge, the length factor itself can mimic the spin of the Kerr black hole up to $a/M \simeq 0.13$ and with the increase of the electric charge, one can mimic up to even higher values of the spin. From the right panel, we observe that the range of mimicking spin by the electric charge is greater for lower values of the parameter l, and in the Reissner–Nordström case, it achieves its peak, up to $a/M \simeq 0.56$.

Table 1. Numerical results for the dependence of the ISCO radius of the accretion disk from spacetime parameters.

$Q\|l$	0.1	0.2	0.3	0.4	0.5	0.6	0.7
0.1	5.979	5.960	5.928	5.883	5.822	5.745	5.647
0.2	5.933	5.914	5.882	5.835	5.773	5.693	5.592
0.3	5.856	5.836	5.802	5.754	5.689	5.605	5.498
0.4	5.746	5.725	5.689	5.637	5.667	5.477	*NB*
0.5	5.599	5.576	5.537	5.480	5.404	5.304	*NB*
0.6	5.411	5.386	5.342	5.278	5.192	*NB*	*NB*
0.7	5.176	5.146	5.095	5.021	*NB*	*NB*	*NB*
0.8	4.879	4.843	4.781	*NB*	*NB*	*NB*	*NB*
0.9	4.498	4.451	*NB*	*NB*	*NB*	*NB*	*NB*

4. Thermal properties of the thin accretion disk around central compact object

The key characteristics of the accretion disk that will be analyzed include the radiant energy flux across the disk, its radiative efficiency, the temperature distribution, and the spectrum of thermal radiation emitted from the disk.

The flux of electromagnetic radiation emitted from the accretion disk is given by the equation below, as discussed in [34, 35]:

$$F(r) = -\frac{\dot{M}_0}{4\pi\sqrt{-g}M^2}\frac{\Omega,\, r}{(E - \Omega L)^2}\int_{r_{\mathrm{ISCO}}}^{r}(E - \Omega L)L_{,r}\,\mathrm{d}r, \quad (7)$$

where g is the determinant of the metric tensor. Next, we explore the electromagnetic radiation flux emitted by an accretion disk surrounding a black hole and determine how this flux varies radially for various values of the spacetime parameters of the black hole. The outcomes are shown in figure 6. Starting from the left panel, it is seen that the increase of the electric charge of a black hole for fixed l increases the flux of the accretion disk only in the near regions around the ISCO and in the further distances the effect weakens fast. It is also seen that for a bigger electric charge, we would have the shift of lines towards the black hole which is related with the decrease of the ISCO radius with the increase of the electric charge of a black hole. These points indeed mark the innermost region of the disk that is visible due to the emitted radiation and define the inner boundary of the accretion disk which can also be observed from (7). From the right plot, we can notice that the increase of the parameter l for the fixed electric charge of a black hole has similar characteristics but with a considerably weak effect.

The ability of the central object to convert accreted material into outgoing electromagnetic radiation is a vital part

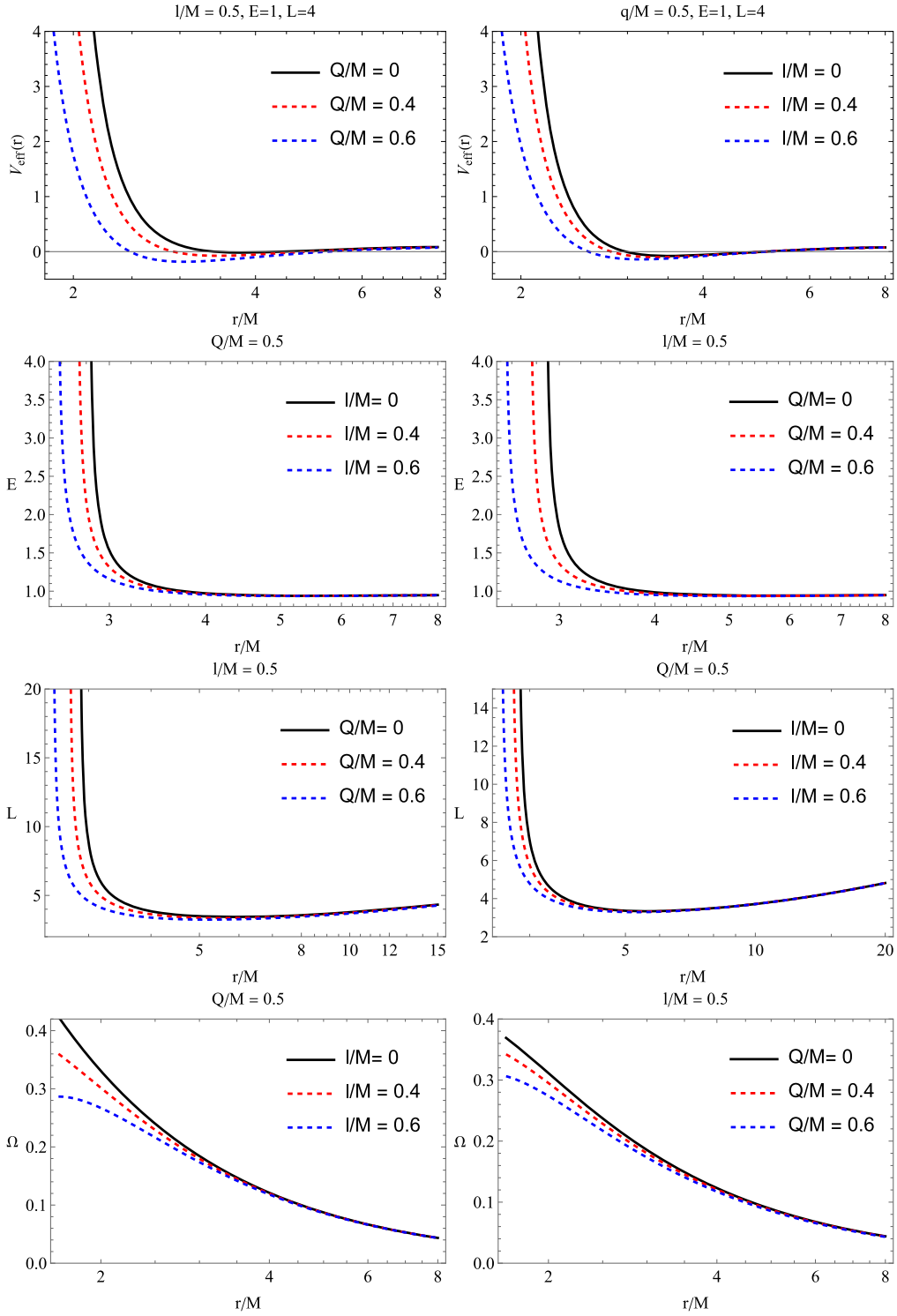

Figure 4. Radial profile of the effective potential, energy and angular momentum for circular motion of a test particle and circular velocity.

of the mass accretion process. The efficiency is defined as the ratio of the rate at which photons emitted from the disk's surface escape to infinity to the rate at which mass-energy is accreted by the central black hole, as explored in earlier works [34, 35]. This efficiency is often expressed in terms of the specific energy at the ISCO [39].

$$\eta = 1 - E_{\rm ISCO}. \tag{8}$$

By utilizing the specific energy relation from (3), we can create a table (see table 2) that provides the corresponding values of η. The data demonstrates that as the electric charge of a black hole increases, the efficiency of the radiation goes up as well. This happens because the increase in the charge weakens the black hole's gravitational field. Since radiative efficiency is related to the energy of photons emitted by the disk and measured at infinity, a weaker gravitational field

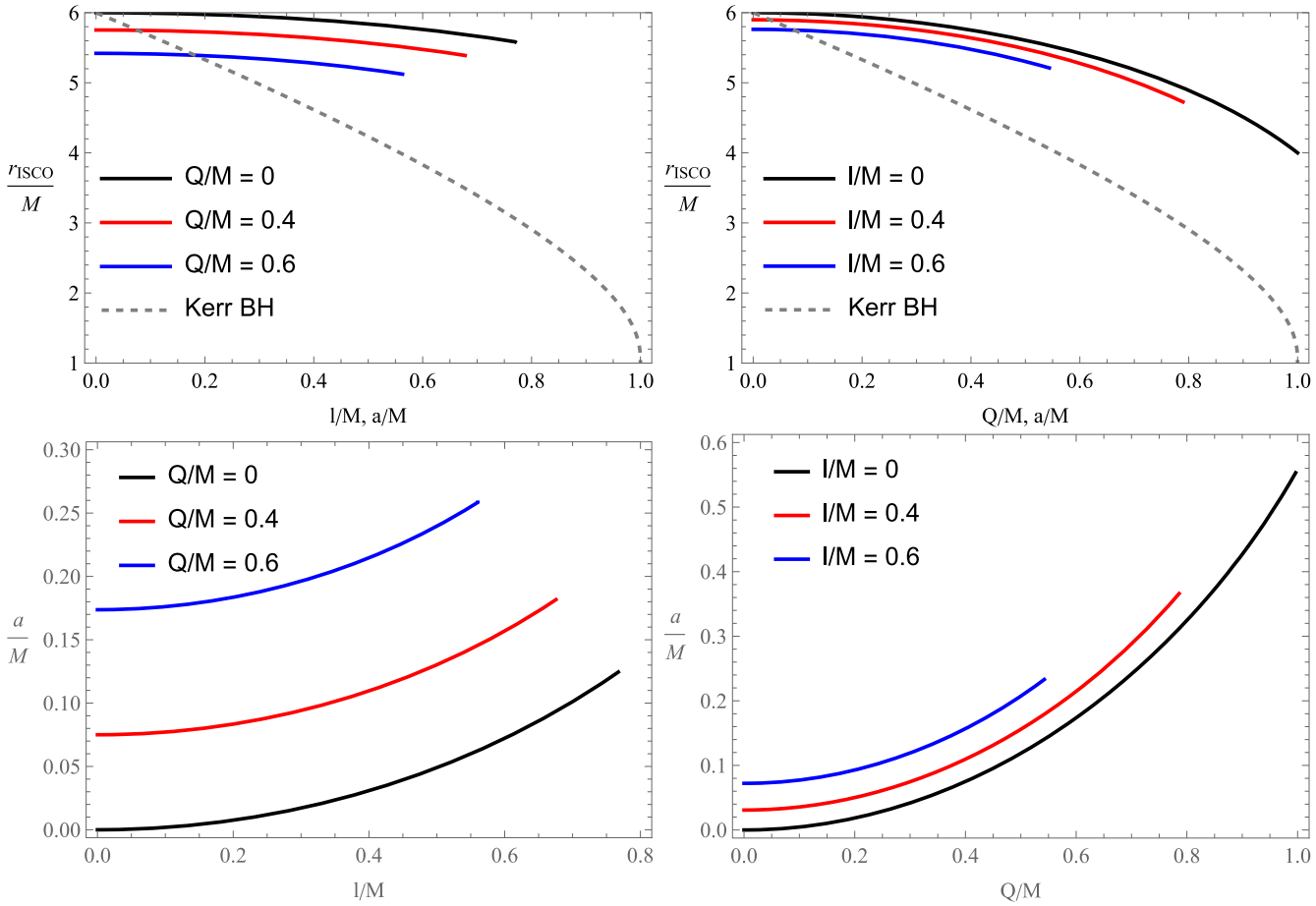

Figure 5. Degeneracy plot showing how well the electric charge Q and length factor l can mimic the spin of rotating Kerr black hole.

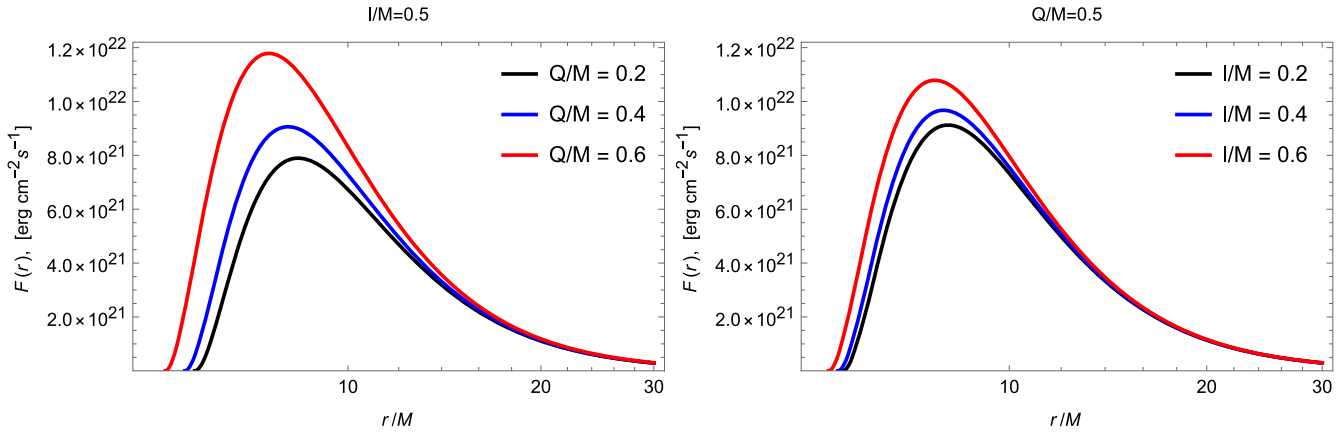

Figure 6. The plot demonstrates how the flux of radiation emitted from the accretion disk changes with the distance from the central compact object for different values of spacetime parameters.

causes the energy of these photons to increase. A similar effect but in a weaker manner can be noticed for the length factor l.

The graphical representation of the results are shown in figure 7. From the left panel, one can state that in the absence of the electric charge of a black hole, the length factor itself can rise the efficiency of the radiation of the disk up to $\eta \simeq 0.6$, while the presence of the former can increase its value notably. In the right panel similar behavior takes place for different l and the smooth change of Q. It can be seen that the effect of the electric charge is considerably stronger than that of the length factor. One can also see that even though the increase of the length factor increases the radiative efficiency for fixed Q, it limits the maximum allowed value of the

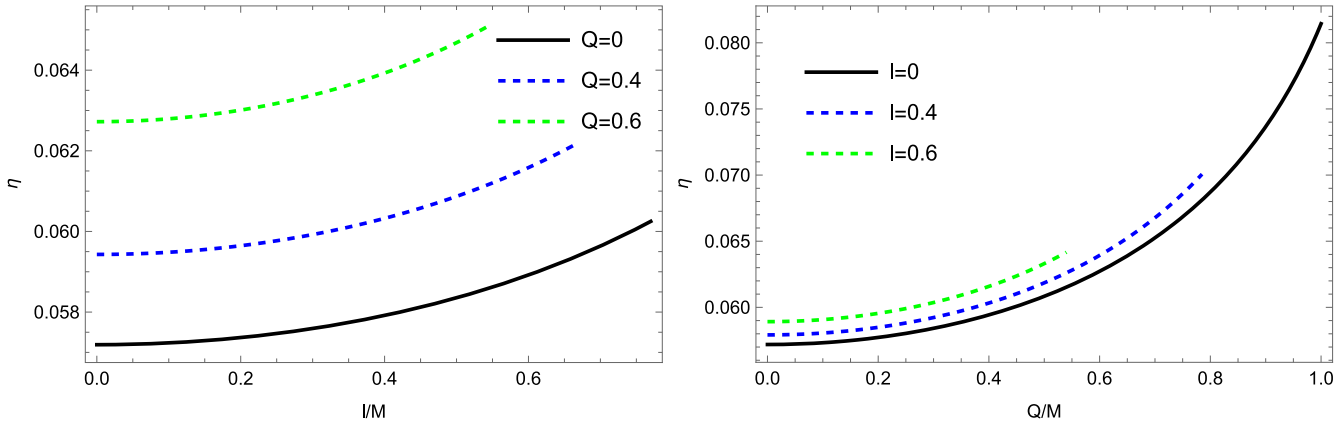

Figure 7. Plots illustrating the change of the efficiency of the radiation of the accretion disk with the change of spacetime parameters.

Table 2. The dependence of the radiative efficiency of the accretion disk from spacetime parameters.

$Q\|l$	0.1	0.2	0.3	0.4	0.5	0.6	0.7
0.1	0.0573	0.0575	0.0577	0.058	0.0585	0.059	0.0598
0.2	0.0577	0.0579	0.0581	0.0584	0.0589	0.0595	0.06
0.3	0.0584	0.0586	0.0588	0.0592	0.0597	0.0603	0.0611
0.4	0.0594	0.0596	0.0599	0.0603	0.0608	0.0615	*NB*
0.5	0.0608	0.061	0.0613	0.0618	0.0624	0.0633	*NB*
0.6	0.0627	0.063	0.0634	0.0639	0.0646	*NB*	*NB*
0.7	0.065	0.0656	0.066	0.0667	*NB*	*NB*	*NB*
0.8	0.069	0.0692	0.0698	*NB*	*NB*	*NB*	*NB*
0.9	0.0738	0.0743	*NB*	*NB*	*NB*	*NB*	*NB*

electric charge and thus in general reduces the maximum efficiency of radiation that can be achieved.

Now, let's analyze the temperature of the disk surrounding the black hole. It should be noted that the previously calculated flux does not represent blackbody radiation alone, but rather the average flux across the disk. This is important because, in the steady-state thin disk model, it is assumed that the accreting matter is in thermodynamic equilibrium. Consequently, the radiation emitted from the disk's surface is modeled as blackbody radiation.

Blackbody radiation describes the electromagnetic radiation emitted by an ideal object that absorbs all incoming radiation and re-emits it, following a spectrum that is solely dependent on the object's temperature. However, in an accretion disk, the emitted radiation is influenced by factors like the disk's temperature and its density, and not strictly described by blackbody radiation. The emission is shaped by various physical phenomena such as Compton scattering, synchrotron radiation, and line emission, making the spectrum deviate from a pure blackbody form.

Despite this, some accretion disk models approximate the emitted radiation as a blackbody spectrum. These models typically assume that the disk is optically thick, remains in local thermal balance, and that the radiation emitted comes from a surface layer in thermal balance with the underlying material. Such models, referred to as 'multi-temperature blackbody' models, offer reasonable approximations of the actual spectrum emitted by the accretion disk.

The flux of blackbody radiation is given by the equation $F = \sigma T^4$, where σ represents the Boltzmann constant. Using this relation, we can generate a radial temperature profile for the disk, as illustrated in the top panels of figure 8. The top-left panel is for fixed length factor and different electric charge while the top-right one for fixed Q and different l. From the panels one can see that both spacetime parameters have similar effects increasing the temperature of the disk in close distance from the central compact object while in far distances their effects are negligible. One noticeable difference between the plots is that the effect of the electric charge is stronger than the length factor as usual. One can translate the temperature of the disk into the average thermal energy of particles in the disk through the relation $E = kT$ (k is a Boltzmann constant) which is shown in the bottom panels of figure 8. The discussion regarding the temperature of the accretion disk applies equally to the energy, as they are linearly proportional.

One can also present the temperature profile of the accretion disk around a black hole in a so called density-plot version as shown in figure 9. We illustrate the variation in temperature of the accretion disk as the radial coordinate changes with respect to electric charge and the length factor, respectively in the top-left and top-right panels. In the plots

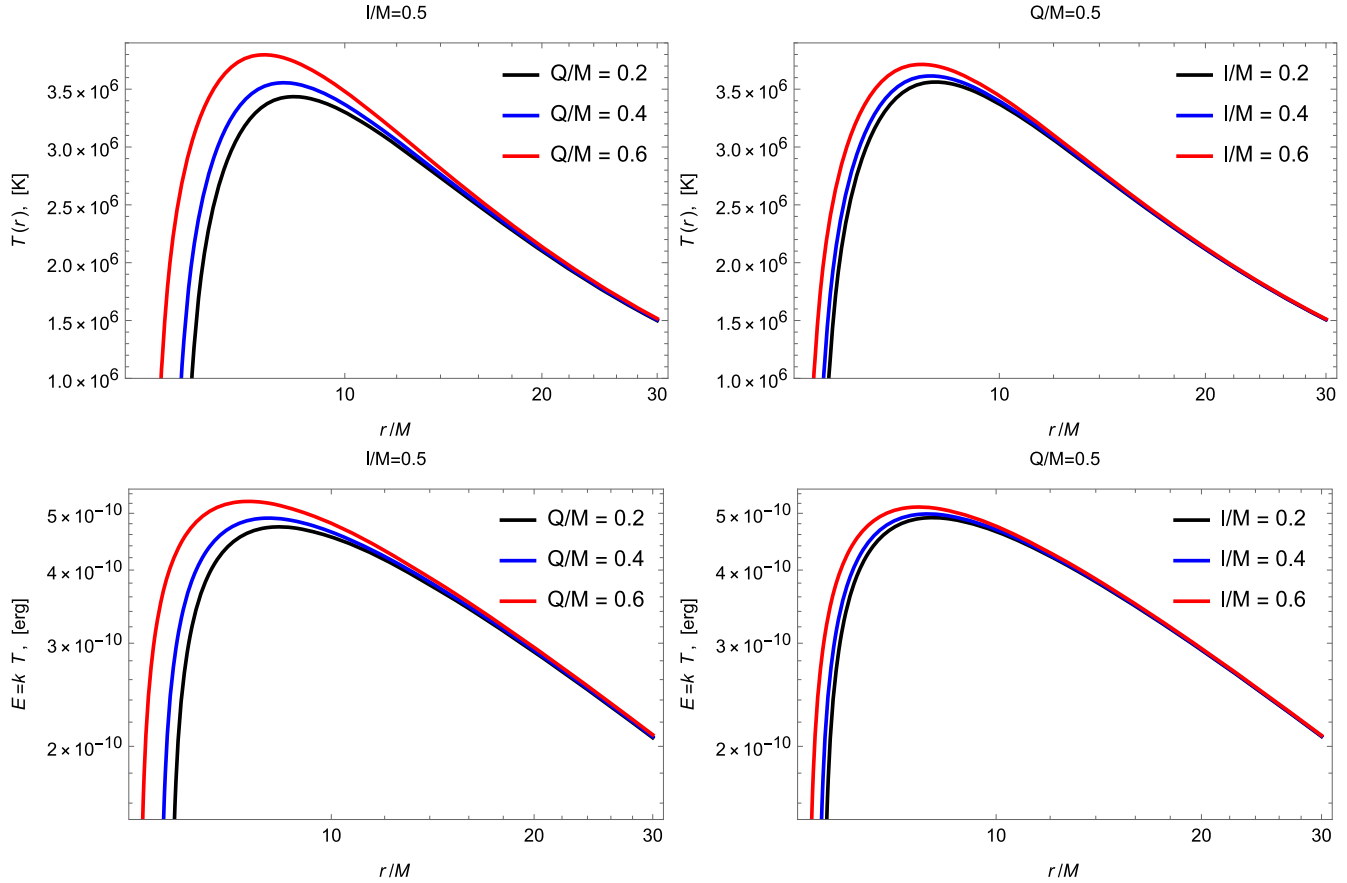

Figure 8. The change of the temperature (top panels) and thermal energy of the particles (bottom panels) of the accretion disk with the radial distance for different values of spacetime parameters.

one can notice violet shaded region whose edge represents the ISCO of test particles in the disk or equalently, the inner edge of the disk according to Novikov–Thorne disk model. From the top-left plot one can state that the temperature becomes higher for a larger electric charge of a black hole for the fixed radial distance from the center. Similar behavior can be observed from the top-right plot but with considerably weaker effect. In the bottom plot we show the change of the temperature with the radial coordinate for the fixed values of spacetime parameters. The central black circle denotes the black hole with its event horizon. The plot effectively demonstrates the realistic temperature profile of the disk. It is evident that the disk's temperature rapidly increases from the inner edge, reaches its peak near the ISCO, and then gradually decreases as it moves farther from the center.

The radiation luminosity can be computed using the formula provided in [40].

$$L(\nu) = 4\pi d_L^2 I(\nu) = \frac{8}{\pi}\cos i \int_{r_{\rm in}}^{r_{\rm ex}} \int_0^{2\pi} \frac{\nu_e r \mathrm{d}\phi \mathrm{d}r}{\mathrm{e}^{(\nu_e/T)} - 1} \quad . \tag{9}$$

Here, d_L represents the distance between the remote source and the observer, with i representing the inclination angle of the accretion disk, r_{in} and r_{ex} correspond to the inner and outer boundaries of the disk, respectively, and $I(\nu)$ is the Planck distribution function. Commonly, $r_{in} = r_{\rm ISCO}$ and $r_{ex} \to \infty$ are selected. The emitted frequency $\nu_e = \nu(1+z)$ is altered by the redshift factor z, which can be expressed as [41].

$$1 + z = \frac{1 + \Omega r \sin\phi \sin i}{\sqrt{-g_{tt} - 2\Omega g_{t\phi} - \Omega^2 g_{\phi\phi}}}. \tag{10}$$

Now, one can analyze the spectrum of the disk as presented in figure 10. It is shown in the left panel that larger values of electric charge of the ECH BH results in higher luminosity of the disk, especially around its peak intensity. The figure reveals that the peak intensity of thermal radiation occurs at approximately $\sim 1.5 \times 10^{17}$ Hz or ~ 0.6, keV, corresponding to electromagnetic radiation within the soft x-ray band. It is also evident that the luminosity of the accretion disk surrounding the ECH BH is consistently higher compared to that of a black hole without electric charge. Additionally, for an electrically charged Hayward black hole, the disk luminosity increases as the parameter Q grows, with the peak of the curves shifting toward higher frequencies. Very similar behavior, but again in a weaker manner, can be observed from the right plot where change of the luminosity of the disk with the change of the frequency of electromagnetic radiation is shown for fixed electric charge Q and various values of the length factor l.

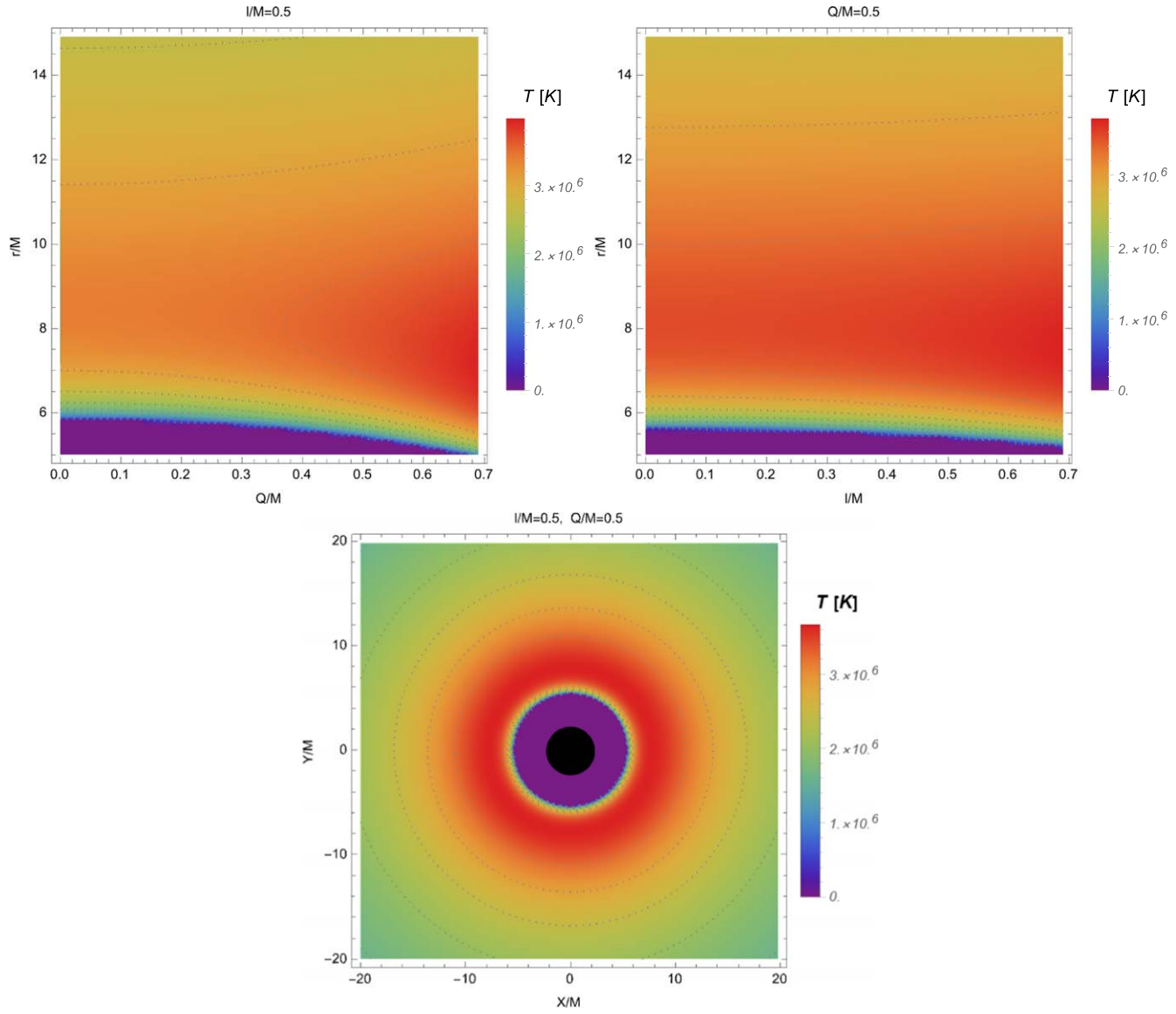

Figure 9. Density-plot version of the obtained results for the temperature of the accretion disk around the ECH BH.

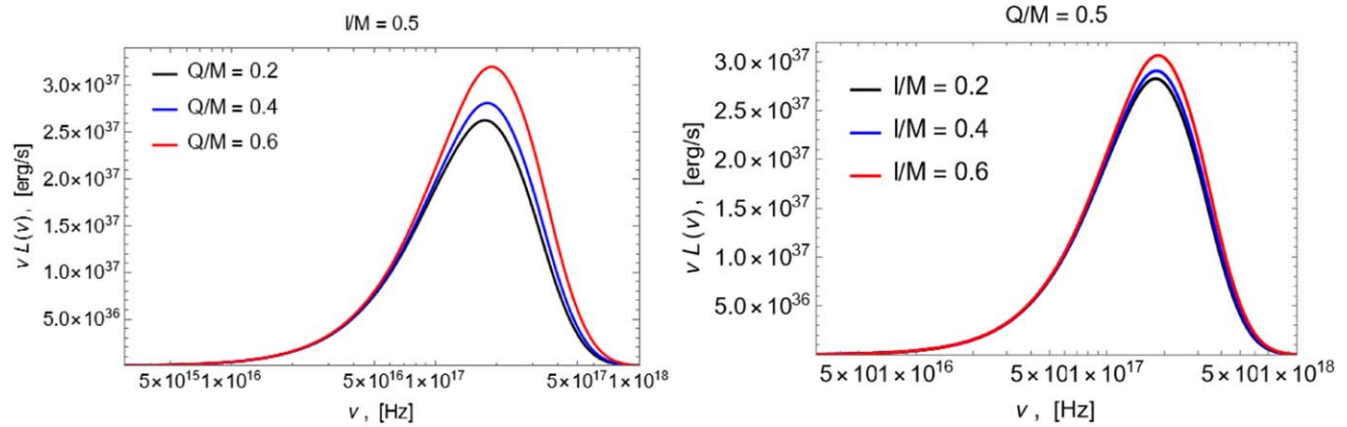

Figure 10. The spectrum of the accretion disk surrounding a black hole for different black hole parameters and fixed angle of inclination at $i = \pi/6$.

5. Summary

In this work, we carried out a comprehensive investigation of charged Hayward black holes, focusing on the properties of accretion disks. Our study highlights the significant influence of both the electric charge Q and the length factor l on the black hole's characteristics, although the electric charge tends to have a stronger effect.

First, we explored how these spacetime parameters affect the structure of the event horizon. Our findings show that increasing either the electric charge or the length factor reduces the size of the event horizon, with the electric charge having a slightly more pronounced effect. Additionally, in the absence of the length factor, the charged Hayward black hole closely resembles the Kerr black hole, where the electric charge can effectively mimic the role of spin. The combination of both parameters allows for even more precise mimicking of Kerr black holes, offering insights into how non-rotating black holes can emulate the properties of rotating ones through charge and length factor adjustments.

We also examined the ISCO radius, a critical parameter in determining the dynamics of matter around black holes. Our results demonstrate that both Q and l reduce the ISCO radius in a manner similar to how spin influences the ISCO in Kerr black holes. The electric charge plays a dominant role, particularly in cases with larger charge values. Notably, the length factor alone can mimic the spin of Kerr black holes up to $a/M \simeq 0.13$, and when combined with the electric charge, it can replicate even higher spin values, enhancing our understanding of how these spacetime parameters govern orbital dynamics near the black hole.

Furthermore, we investigated the accretion disk's radiation flux and found that increasing the electric charge enhances the flux near the ISCO, while the effect diminishes at greater radial distances. The length factor also affects the flux, though its influence is notably weaker. This behavior is mirrored in the temperature profile of the accretion disk, where the temperature peaks near the ISCO and gradually decreases as one moves farther from the black hole. The electric charge raises the disk temperature more significantly than the length factor, indicating that charged black holes can have a stronger effect on the thermal dynamics of the surrounding disk.

The radiative efficiency of the accretion disk, a key measure of how efficiently matter is converted into electromagnetic radiation, follows a similar trend. Both parameters increase the efficiency, with the electric charge having a more substantial impact. The length factor, while still contributing to higher efficiency, limits the maximum value of the electric charge, thus constraining the overall maximum efficiency that can be achieved.

Lastly, we analyzed the electromagnetic spectrum of the disk's radiation and discovered that the peak intensity of thermal radiation occurs around $\sim 1.5 \times 10^{17}$ Hz or ~ 0.6 keV, which corresponds to soft x-ray emissions. The luminosity of the disk was consistently higher for black holes with nonzero electric charge compared to neutral ones. As the electric charge increases, the disk's luminosity rises, and the peak shifts toward higher frequencies, demonstrating the impact of Q on the radiative output. The length factor, while producing similar behavior, does so with less intensity. These findings underline the strong influence of electric charge on the disk's thermal spectrum and luminosity, while also highlighting the subtler role of the length factor.

In conclusion, our study reveals that charged Hayward black holes exhibit a rich and complex structure, with both the electric charge and length factor playing crucial roles in shaping the black hole's event horizon, ISCO, and accretion disk properties. The electric charge emerges as the dominant factor influencing the gravitational and radiative characteristics of the system, while the length factor provides similar influence but with less strength. Together, these parameters offer new perspectives on the dynamics of non-rotating and charged black holes, as well as the astrophysical phenomena occurring in their vicinity. These insights can be particularly useful for understanding black holes in modified gravity theories and their observational signatures, especially in x-ray astronomy.

References

[1] Penrose R 1965 Gravitational collapse and space-time singularities *Phys. Rev. Lett.* **14** 57–9

[2] Hawking S 1967 The occurrence of singularities in cosmology. III. Causality and singularities *Proc. Roy. Soc. Lond.* A **300** 187–201

[3] Hawking S W and Penrose R 1970 The Singularities of gravitational collapse and cosmology *Proc. Roy. Soc. Lond.* A **314** 529–48

[4] Newman E, Tamburino L and Unti T 1963 Empty space generalization of the Schwarzschild metric *J. Math. Phys.* **4** 915

[5] Misner C W 1963 The Flatter regions of Newman, Unti and Tamburino's generalized Schwarzschild space *J. Math. Phys.* **4** 924–38

[6] Lynden-Bell D and Nouri-Zonoz M 1998 Classical monopoles: Newton, NUT space, gravimagnetic lensing and atomic spectra *Rev. Mod. Phys.* **70** 427–46

[7] Ayón-Beato E and Garcìa A 1998 Regular black hole in general relativity coupled to nonlinear electrodynamics *Phys. Rev. Lett.* **80** 5056–9

[8] Ayon-Beato E and Garcia A 1999 Nonsingular charged black hole solution for nonlinear source *Gen. Rel. Grav.* **31** 629–33

[9] Ayon-Beato E and Garcia A 2000 The Bardeen model as a nonlinear magnetic monopole *Phys. Lett.* B **493** 149–52

[10] Dymnikova I 1992 Vacuum nonsingular black hole *Gen. Rel. Grav.* **24** 235–42

[11] Dymnikova I 2004 Regular electrically charged structures in nonlinear electrodynamics coupled to general relativity *Class. Quant. Grav.* **21** 4417–29

[12] Bronnikov K A 2001 Regular magnetic black holes and monopoles from nonlinear electrodynamics *Phys. Rev.* D **63** 044005

[13] Bronnikov K A and Fabris J C 2006 Regular phantom black holes *Phys. Rev. Lett.* **96** 251101

[14] Berej W, Matyjasek J, Tryniecki D and Woronowicz M 2006 Regular black holes in quadratic gravity *Gen. Rel. Grav.* **38** 885–906

[15] Burinskii A and Hildebrandt S R 2002 New type of regular black holes and particlelike solutions from nonlinear electrodynamics *Phys. Rev.* D **65** 104017
[16] Ansoldi S 2008 Spherical black holes with regular center: a review of existing models including a recent realization with Gaussian sources arXiv:0802.0330
[17] Ashtekar A and Bojowald M 2005 Black hole evaporation: a paradigm *Class. Quant. Grav.* **22** 3349–62
[18] Hayward S A 2006 Formation and evaporation of nonsingular black holes *Phys. Rev. Lett.* **96** 031103
[19] Guo S, Li G-R and Liang E-W 2022 Influence of accretion flow and magnetic charge on the observed shadows and rings of the Hayward black hole *Phys. Rev.* D **105** 023024
[20] Kocherlakota P *et al* 2021 Constraints on black-hole charges with the 2017 EHT observations of M87* *Phys. Rev.* D **103** 104047
[21] Hakimov A, Abdujabbarov A and Narzilloev B 2017 Quantum interference effects in conformal Weyl gravity *Int. J. Mod. Phys.* A **32** 1750116
[22] Rayimbaev J, Narzilloev B, Abdujabbarov A and Ahmedov B 2021 Dynamics of magnetized and magnetically charged particles around regular nonminimal magnetic black holes *Galaxies* **9**
[23] Narzilloev B, Rayimbaev J, Abdujabbarov A and Ahmedov B 2021 Regular Bardeen black holes in Anti-de Sitter spacetime versus Kerr black holes through particle dynamics *Galaxies* **9**
[24] Narzilloev B and Ahmedov B 2022 Radiation properties of the accretion disk around a black hole surrounded by PFDM *Symmetry* **14**
[25] Narzilloev B and Ahmedov B 2023 Observational and energetic properties of astrophysical and galactic black holes *Symmetry* **15** 293
[26] Narzilloev B, Abdujabbarov A and Hakimov A 2022 Redshift of photons emitted from the accretion disk of a regular black hole surrounded by dark matter *Int. J. Mod. Phys.* A **37** 2250144
[27] Mirzaev T, Li S, Narzilloev B, Hussain I, Abdujabbarov A and Ahmedov B 2023 Simulated image of the shadow of the Kerr–Newman-NUT–Kiselev black hole in the Rastall gravity with a thin accretion disk *Eur. Phys. J. Plus* **138** 47
[28] Narzilloev B and Ahmedov B 2023 The eye of the storm: Optical properties *Int. J. Mod. Phys.* A **38** 2350026
[29] Abdulxamidov F, Benavides-Gallego C A, Narzilloev B, Hussain I, Abdujabbarov A, Ahmedov B and Xu H 2023 Dynamics of spinning test particles around the Kerr–Newman-NUT black hole with quintessence in the Rastall gravity *Eur. Phys. J. Plus* **138** 635
[30] Alibekov H, Narzilloev B, Abdujabbarov A and Ahmedov B 2023 Frequency shift of photons in the spacetime of deformed RN BH *Symmetry* **15** 1414
[31] Alloqulov M, Narzilloev B, Hussain I, Abdujabbarov A and Ahmedov B 2023 Energetic processes around electromagnetically charged black hole in the Rastall gravity *Chin. J. Phys.* **85** 302–17
[32] Narzilloev B and Ahmedov B 2023 Thermal radiation of thin accretion disk around Taub-NUT black hole *Int. J. Mod. Phys.* D **32** 2350064
[33] Frolov V P 2016 Notes on nonsingular models of black holes *Phys. Rev.* D **94** 104056
[34] Novikov I D and Thorne K S 1973 Astrophysics and black holes *Les Houches Summer School of Theoretical Physics (Les Houches, France, August, 1972)* 343–550
[35] Page D N and Thorne K S 1974 Disk-accretion onto a black hole. time-averaged structure of accretion disk *Astrophys. J.* **191** 499–506
[36] Shapiro S L 2005 Spin, accretion and the cosmological growth of supermassive black holes *Astrophys. J.* **620** 59–68
[37] Shakura N I and Sunyaev R A 1973 Black holes in binary systems. observational appearance *Astron. Astrophys.* **24** 337–55
[38] Banerjee I, Chakraborty S and SenGupta S 2019 Decoding signatures of extra dimensions and estimating spin of quasars from the continuum spectrum *Phys. Rev.* D **100** 044045
[39] Thorne K S 1974 Disk-accretion onto a black hole. II. evolution of the hole *Astrophys. J.* **191** 507–20
[40] Torres D F 2002 Accretion disc onto a static non-baryonic compact object *Nucl. Phys.* B **626** 377–94
[41] Bhattacharyya S, Misra R and Thampan A V 2001 General relativistic spectra of accretion disks around rotating neutron stars *Astrophys. J.* **550** 841–5